Atmos. Chem. Phys. Discuss., 3, 2353–2391, 2003
www.atmos-chem-phys.org/acpd/3/2353/

Atmospheric Chemistry and Physics Discussions

Characteristics, impacts and direct radiative forcing of aerosols at the ARM Southern Great Plains Central Facility

M. G. Iziomon and U. Lohmann

Department of Physics and Atmospheric Science, Dalhousie University, Halifax, Canada

Received: 3 February 2003 – Accepted: 18 April 2003 – Published: 13 May 2003

Correspondence to: M. G. Iziomon (iziomon@mathstat.dal.ca)

Abstract

Based on the analysis of five years of field measurements of aerosol and meteorological variables, we present the characteristics, impacts and direct radiative forcing of aerosols at the Southern Great Plains (SGP) Central Facility (CF) of the Atmospheric Radiation Measurement (ARM) Program. Annual means of total submicron aerosol concentration for particles with aerodynamic diameter (Dp) $< 1\,\mu$m, particle concentration (N_p) for aerosols with $0.1 \leq D_p \leq 10\,\mu$m, submicron light absorption coefficient (σ_a) and single scattering albedo at the SGP CF amount to $5306 \pm 392\,\mathrm{cm}^{-3}$, $654 \pm 290\,\mathrm{cm}^{-3}$, $2.0 \pm 0.7\,\mathrm{Mm}^{-1}$ and 0.94 ± 0.02, respectively, while those of submicron total scattering coefficient, hemispheric backscatter fraction, submicrometer scattering fraction (R_{sp}), Ångström exponent, hygroscopic growth factor and visibility at 550 nm are $36 \pm 2\,\mathrm{Mm}^{-1}$, 0.12 ± 0.01, 0.84 ± 0.03, 2.25 ± 0.09 and 1.84 ± 0.10, 38 ± 2 km, respectively. Although they exhibit a considerable year-to-year variability, R_{sp}, σ_a, N_p and ozone show some increase over the period examined here. This increase is accompanied by a decline in annual precipitation, column integrated water vapor, relative humidity, and cloud cover (particularly from 1998 to 2001) at the site. In particular, the marked precipitation deficit at the SGP CF in 2000 and 2001 is evident of drought associated with La Nina conditions. We compare the diabatic impacts and optical characteristics for smoke and dust aerosols. In general, aerosols at the ARM site produce a net diabatic cooling, with an estimated direct radiative forcing ranging from about $-0.7\,\mathrm{W\,m}^{-2}$ in winter to $-2.4\,\mathrm{W\,m}^{-2}$ in summer.

1. Introduction

Aerosols in the atmosphere (which include sulfate, black carbon, organic carbon, mineral dust, sea-salt, volcanic ash and pollen) evolve in size and composition by homogenous and heterogeneous nucleation, condensation, coagulation as well as dry and wet

ACPD

3, 2353–2391, 2003

deposition. By influencing the geochemical and hydrological cycles as well as the surface radiation budget, aerosols exhibit a significant impact on the Earth's climate.

On one hand, aerosols absorb and scatter radiation (direct aerosol effect). On the other hand, they act as cloud condensation nuclei and thus determine the initial cloud droplet number concentration, cloud albedo, precipitation efficiency and cloud lifetime (indirect aerosol effect) (Twomey, 1991; Lohmann et al., 2000; Bréon et al., 2002). Hansen et al. (1997) hypothesized that the absorption of solar radiation by black carbon (BC) within a cloud or in a clear region can result either in a local reduction of cloud cover fraction A_c or can inhibit cloud formation, respectively (semi-direct aerosol effect). Although an increase in cloud liquid water path owing to aerosols has been observed by some investigators (e.g. Radke et al., 1989), other observations suggest that this effect is insignificant (Platnick et al., 2000; Leaitch et al., 1992; Nakajima et al., 2001). Consequently, the impact of increased aerosols on cloud cover and cloud water content is still unclear (Nakajima et al., 2001). Furthermore, while aerosols may produce a net atmospheric cooling in some regions, other regions may experience a net heating, and the long-term climatic impact of these changes are not well known (Penner et al., 1994; Haywood et al., 1999).

Aerosol campaigns such as the Southern African Regional Science Initiative (SAFARI) (Le Canut et al., 1996; Andreae et al., 1996), Transport and Atmospheric Chemistry near the Equatorial Atlantic (TRACE A) (Anderson et al., 1996), Smoke, Clouds, and Radiation-Brazil (SCAR-B) (Kaufmann et al., 1998), Indian Ocean Experiment (INDOEX) (Lelieveld et al., 2001), Large-scale Biosphere-Atmosphere Experiment in Amazonian – Cooperative LBA Airborne Regional Experiment 98 (LBA-CLAIRE-98) (Andreae et al., 2001) have provided samples of tropical biomass burning aerosol size distributions from aircraft measurements. However, aerosol type and size distributions vary considerably in space and time. While aircraft measurements are particularly suited for the resolution of the vertical profile of aerosols, the aerosol burden above or below the aircraft level legs is generally either estimated or ignored (Ross et al., 1998; Remer et al., 1998). Furthermore, aircraft aerosol measurements only cover a rela-

ACPD
3, 2353–2391, 2003

tively short period. The long-term measurement of aerosols and cloud properties as well as meteorological conditions provides a formidable way of characterizing aerosols, evaluating the climatic impact of aerosols and thus reducing the high uncertainties associated with aerosols in climate forcing assessments.

The U. S. Southern Great Plains (SGP) Cloud and Radiation Testbed was the first and largest field measurement site established by the Atmospheric Radiation Measurement (ARM) Program for the measurement of radiation, cloud, aerosol and atmospheric properties. The SGP Cloud and Radiation Testbed covers an area of approximately 142, 450 km^2 in north central Oklahoma and south central Kansas (see Fig. 1). The central facility (CF) of the SGP Cloud and Radiation Testbed is located on 65 hectares of cattle pasture and wheat fields southeast of Lamont, Oklahoma (36.60° N, 97.50° W, 315 m a.s.l.). Sheridan et al. (2001) presented aerosol measurement at the SGP CF for aerosols with aerodynamic diameter less than 10 μm. Here, we focus particularly on submicron aerosols and their impact on atmospheric properties. We investigate the variability of submicron aerosols at the SGP CF, examine plausible feedback mechanisms between aerosol variation and atmospheric processes as well as estimate the net diabatic impact and direct radiative forcing of aerosols at the ARM site.

2. Field measurements at the Southern Great Plains Central Facility

The Aerosol Observing System at the SGP CF is the major ARM platform for conducting in-situ aerosol measurements at 10 m above the surface since April 1996. The NOAA Climate Monitoring and Diagnostics Laboratory (CMDL) in Boulder Colorado operates the Aerosol Observing System. In early 2000, an aerosol filter sampling system was added to collect particles for subsequent physical and chemical analysis. The Aerosol Observing System measures the optical properties of ambient aerosol particles obtained from the top of a≈21.4 cm inner diameter stainless steel intake stack. Aerosol optical properties measured include light absorption coefficient (σ_a) in m^{-1}, total light scattering coefficients (σ_s) in m^{-1}, hemispheric backscattering coefficients (σ_b)

ACPD
3, 2353–2391, 2003

in m^{-1}, total number concentration of condensation particles (N_a) in cm^{-3} and number concentration for particles of size ranging from 0.1–10 μm diameter (N_p) in cm^{-3}. In addition, measurements of the aerosol scattering coefficient as a function of relative humidity ($f(RH) = \sigma_{s(RH=85\%)}/\sigma_{s(RH=40\%)}$) commenced at the SGP CF in December 1998. The Dasibi (Model 1008) ozone monitor at the SGP CF measures ozone mixing ratios between 1 to 1000 ppbv, using monochromatic ultraviolet absorption spectrophotometry.

σ_s and σ_b at three wavelengths (450, 550, and 700 nm) are measured by a TSI nephelometer. σ_s as a function of relative humidity at three wavelengths (450, 550, and 700 nm) is measured by a system of two TSI nephelometers connected to a humidity scanning system (Anderson and Ogren, 1998). σ_a is measured using a filter-based radiance research particle soot absorption photometer (PSAP), which is calibrated to estimate suspended-state aerosol light absorption at 550 nm using an extinction cell and a nephelometer (Bond et al., 1999). N_a is measured by a TSI condensation nuclei counter (CNC) while N_p is measured by an optical particle counter (OPC).

The aerosol sample stream is conditioned to be lower than 40% relative humidity before it enters the sampling lines, and subsequently into the instruments. Size-segregated measurements of σ_s and σ_a were made through a switch impactor system, such that only particles with aerodynamic diameter D_p smaller than 10 μm were sampled, with a 1 μm alternate size and a 10 μm default size cut. Except for N_p and where otherwise stated, the aerosol optical properties examined here are associated with submicron aerosols with $Dp < 1\,\mu$m at 550 nm.

We derive intensive aerosol optical quantities including the hemispheric backscatter fraction b, single scattering albedo ω_0, Ångström exponent å and submicrometer scattering fraction R_{sp} as follows:

$$b = \sigma_b/\sigma_s, \quad (1)$$

$$\omega_0 = \sigma_s/(\sigma_s + \sigma_a), \quad (2)$$

$$\mathring{a} = -\log[\sigma_s(\lambda_1)/\sigma_s(\lambda_2)]/\log[(\sigma_1)/(\lambda_2)], \quad (3)$$

ACPD
3, 2353–2391, 2003

$$R_{sp} = [\sigma_s(D_p < 1\,\mu\text{m})/\sigma_s(D_p < 10\,\mu\text{m})]. \quad (4)$$

In March 2000, a joint project between the ARM program and the Climate Monitoring and Diagnostics Laboratory (CMDL) to obtain a statistically significant data set of the vertical distribution of aerosol properties commenced. The aerosol measurements are made by flying a light aircraft (Cessna C-172N) over the SGP site and utilizing an aerosol instrument package similar to the one used for surface measurements. The aircraft flies level legs at altitudes between 500 m and 3500 m.

The ARM Microwave Water Radiometer (MWR) measures column-integrated amounts of water vapor and liquid water. The MWR (model WVR-1100) receives microwave radiation from the sky at two frequencies (23.8 GHz and 31.4 GHz), which allow simultaneous determination of water vapor and liquid water burdens along a selected path. Column integrated precipitable water vapor PWV and cloud liquid water path LWP are then given as

$$PWV = (1/\rho_{\text{wt}}) \int \rho_{\text{v}}(\text{z})\,\text{dz}, \quad (5)$$

$$LWP = (1/\rho_{\text{wt}}) \int w_{(\text{z})}\,\text{dz}, \quad (6)$$

where ρ_{wt} is the density of liquid water, ρ_{v} (z) is the vertical distribution of water vapor density and w (z) is the vertical distribution of cloud liquid water content. Here we express PWV in cm and LWP in g m^{-2}. LWPs recorded during periods of precipitation are excluded from our analysis. The ARM surface meteorology observation system (SMOS) provides measurements of meteorological variables including air temperature T_a, relative humidity RH, wind speed v, wind direction and precipitation P_p. Shortwave and longwave radiation at the SGP CF are measured by the ARM solar infrared radiation station. The raw sampling interval of most ARM surface data is 1 min. We utilize ARM data averaged hourly for a period ranging from 1997 to 2001.

The Atmospheric Emitted Radiance Interferometer (AERI) measures the absolute infrared spectral radiance of the sky directly above the instrument every 10 min. Among

ACPD
3, 2353–2391, 2003

others, the AERI data can be used for evaluating line-by-line radiative transport codes and calculating vertical atmospheric profiles of temperature and water vapor. The Raman Lidar is an active, ground-based laser remote sensing instrument that measures vertical profiles of water-vapor mixing ratio r as well as several cloud and aerosol related quantities.

In order to complement field measurements, weather conditions at the SGP central facility are recorded hourly by trained operators throughout periods of intensive operation and usually from 04:30 to 08:30 and from 10:30 to 22:30 UTC on workdays. Recorded weather conditions by ARM trained observers include cloud cover fraction as well as the presence of smoke, dust and fog in the atmosphere. We obtained ARM Metadata weather records for the period 1997 to 2001.

3. Meteorological conditions at the Southern Great Plains Central Facility

In view of its mid-latitude location and continental position, SGP records a wide range of thermodynamic, moisture and cloud fields. Figure 2 presents the annual variation of air temperature, precipitable water vapor, liquid water path, cloud fraction, wind speed and precipitation at the central facility. The bottom and top bars in Fig. 2 represent the lowest and highest monthly mean from 1998 to 2001 while the data points represent the overall monthly mean over this period. Surface air temperature and PWV exhibit a typical mid-latitude annual variation, with mean values ranging, respectively, between $2 - 6^{\circ}$ C and 1.1 – 1.2 cm in winter, and $24 - 29^{\circ}$ C and 3.6 – 4.2 cm in summer. LWP, cloud fraction, wind speed and precipitation are relatively small in late summer (August). The annual mean of T_a, PWV, LWP, A_c, v, P_p at the site are $15.2 \pm 0.4^{\circ}$ C, 2.3 ± 0.1 cm, 54.6 ± 4.1 g m^{-2}, $45 \pm 4\%$, 5.6 ± 0.1 m s^{-1} and 2.33 ± 0.63 mm d^{-1}, respectively. The most dominant wind direction at the ARM site is southerly.

ACPD
3, 2353–2391, 2003

4. Results and discussion

4.1. Aerosol variation at the Southern Great Plains Central Facility

Diurnal variations of aerosol optical properties are capable of providing insight into the processes responsible for new particle formation and convective transport (Weingartner et al., 1999). The seasonal mean diurnal variation of aerosol optical properties at the SGP CF (averaged from 1997 to 2001) is presented in Fig. 3. Meteorological seasons are implied here (i.e. winter: December to February, spring: March to May, summer: June to August and autumn: September to November). N_a shows a pronounced and consistent diurnal cycle during all the seasons. The lowest mean hourly N_a is observed in the morning while peak values were recorded at 17:00 UTC (11:00 LT) during summer and between 19:00 and 21:00 UTC during winter, spring, and autumn. The diurnal maximum of N_a recorded around local noon at the SGP CF is suggestive of a thermally driven aerosol production. The onset of solar radiation in the morning triggers the photochemical production of new particles (Weber et al., 1997). However, these particles, whose formation also depends on the concentration of precursor gases and ions, are only detected later by the condensation nuclei counter when they exceed the lower size detection limit (Weingartner et al., 1999). In addition, the afternoon maximum of N_a could be associated with a low frequency of precipitation (see Fig. 4) and hence less scavenging of aerosol particles.

σ_s, σ_a and N_p, whose highest hourly values are recorded in summer, exhibit a strong diurnal pattern. In particular, σ_a, σ_s and N_p show higher values in the morning and a broad minimum in the afternoon. The afternoon minimum in σ_a, σ_s and N_p could be related to the diurnal cycle of the relative humidity, since small RH in the afternoon would decrease σ_s and σ_a. In all the seasons, ω_0 rises gradually from 00:00 UTC, reaches a maximum between 12:00 and 18:00 UTC and then falls. This suggests that the aerosols at the SGP CF are more absorbing in the afternoon and evening hours. Hourly values of ω_0 are lowest in autumn and highest in winter. Since the wind direction is mainly southerly in all four seasons, the low values of ω_0 in the autumn, is probably

ACPD
3, 2353–2391, 2003

not due to atmospheric flow, but could be due to absorbing aerosols associated with agricultural activities (among others) near the ARM site. In contrast to σ_s, b shows a minimum between 12:00 and 15:00 UTC in all the seasons. There is a similarity in the diurnal cycles of total light scattering coefficients and Ångström exponent. R_{sp}, which does not vary much over the course of the day, ranges generally between 0.80 and 0.85. This suggests that submicrons aerosols dominate the scattering process for all hours over the seasons.

Figure 5 presents the smoothed annual variation (monthly mean and standard deviation of daily values) of aerosol optical properties (at 550 nm wavelength) at SGP CF (averaged from 1997 to 2001) while Table 1 presents the seasonal median of the variables (at all measured wavelengths). It is noteworthy that the highest monthly mean values of σ_s, σ_a and N_p are recorded in July/August, when aerosol levels are high. In addition, submicron aerosol concentration is appreciable in spring and autumn at the SGP CF (as indicated by the magnitude of N_a) and low in the winter months. It is also remarkable that the monthly means of å and b exhibit a maximum in spring and autumn (with the later dominating) and low values in winter, while ω_0 shows a dip in autumn (October). Thus aerosol sizes at the SGP are smallest in October and largest in winter. One implication of this is that, relative to other seasons, the atmosphere over the SGP in winter is cleaner.

Reduced visibility is the most commonly detectable effect of particles in the atmosphere. The standard visibility V_s is inversely proportional to the extinction coefficient σ_e (in km^{-1}), and is given by the Koshmeider equation as $V_s = K/\sigma_e$, where K is the Koshmeider constant (Koshmeider, 1926). For the 75th percentile value of V_s, K = 1.9 (Griffin, 1980; Ozkaynak et al., 1985). The mean V_s is 0.76 of the 75th percentile (Husar et al., 1979; Schichtel, 2001). Based on the Koshmeider equation, the estimated mean visibility of aerosols at the SGP CF in winter is 40 km, but 32 km in the summer. Relative to winter, aerosol pollution and lower visibility in the summer at the SGP site, could be due to a number of factors including agricultural field burning activities, smoke from remote forest fires, wind-enhanced dust episodes, as well as emissions from auto-

ACPD
3, 2353–2391, 2003

mobiles, oil refineries and power plants. In particular, biomass burning activities at the SGP CF are more pronounced in May, June and July (Iziomon and Lohmann, 2003). In addition, high amounts of airborne dust in summer over the Southeast U.S. have been reported by Prospero (1999). We shall explore the properties and effects of smoke and dust aerosols at the SGP CF in the next section.

The monthly standard deviation (which here is a measure of the variability of measured aerosol optical properties for a particular month from the monthly mean throughout a five year period) is somewhat substantial for some months. This is attributable to the marked temporal variation of aerosol properties. High standard deviation for aerosol optical properties also abounds at other locations and is common (see, for example, Horvath et al., 1993; Bergin et al., 2001; Quinn et al., 2000; Dubovik et al., 2002). However, relative to most aerosol measurements in literature (which are short-spanned), the length of data considered here is sufficiently long enough to give a representative picture of aerosol characteristics at a typical mid-latitude continental site. Literature values on the spectral dependence of aerosol optical properties are sparse and there is still need for a consensus among the few published results (Kaufman et al., 1998). As shown in Table 1, σ_s and R_{sp} decrease with wavelength at the SGP while b increases with it. The latter is in agreement with Hobbs et al. (1997) and Remer et al. (1998), who also reported an increase in the backscattering coefficient with wavelength in Brazil.

To further put the observed aerosol optical properties at the SGP CF into perspective, Table 2 compares the mean σ_a, σ_s, b, å, ω_0 and f(RH) for June and July at the ARM site with those measured over the same period (except for Linan, China) during some major aerosol field campaigns. The gaps in Table 2 imply missing data. Aerosol measurements at Sagres, Portugal, were carried out from 15 June to 25 July 1997 during the North Atlantic Aerosol Characterization Experiment (ACE-2) (Carrico et al., 2000; Russell et al., 2002). ACE 2 sampled a variety of air masses including Atlantic, polar (north of Arctic circle) and Western European (Quinn et al., 2000). Bergin et al. (2001) and Xu et al. (2002) measured aerosol optical properties in June 1999 at

ACPD
3, 2353–2391, 2003

Beijing, China (a large urban area) and in November 1999 at Linan, China (a rural location), respectively. Aerosol measurements at Cape Grim, Australia were taken during the first aerosol characterization experiment (ACE1) from 15 November to 15 December 1995 (southern hemisphere summer) (Carrico et al., 1998; Quinn et al., 1998). ACE 1 focused on remote marine aerosol minimally perturbed by continental sources (Quinn et al., 2000). The Tropospheric Aerosol Radiative Forcing Observational Experiment (TARFOX) was conducted off the mid-Atlantic coast of the United States in July, 1996 (Kotchenrurther et al., 1999).

Mean σ_s at the SGP CF are higher than those measured at the relatively clean marine locations but slightly lower than that recorded at the land-site of Sagres, which receives anthropogenically perturbed air masses from Europe. As indicated by its slightly higher å, it follows that the aerosols at Sagres are finer and that the location is more anthropogenically influenced than the ARM site. σ_a and σ_s at the SGP are much lower than those recorded in Linan and Beijing, signifying a major anthopogenic influence at the latter locations. In particular, the extremely high absorption coefficient recorded in Beijing is attributed mainly to emissions of elemental carbon from diesel engines (Xu et al., 2002). This is also evident by the very low ω_0 value of 0.81 in Beijing relative to a mean value of 0.94 observed at the ARM site. Low ω_0 values have also been recorded at other locations with high level of industrial pollution/biomass burning, including Mexico city (ω_0 = 0.90) Maldives (INDOEX; aerosol transported largely from the Indian subcontinent) (ω_0 = 0.89), Zambia (African Savanna) (ω_0 = 0.88), Athens, Greece (ω_0 = 0.88) and Tokyo, Japan (ω_0 = 0.77) (Scheff and Valiozis, 1990; Horvath, 1993; Vasilyev et al., 1995; Baumgardner et al., 2000; Eck et al., 2001; Dubovik et al., 2002). Thus in general, aerosol single scattering albedo at the ARM site could be considered intermediate relative to other continental sites. ω_0 at the ARM site is lower than that reported for the marine locations in Table 2. The high ω_0 at the marine sites indicates that the aerosols are well aged and have not been near land for many days prior to being sampled on the ship (Quinn et al. 1998). The Ångström exponent at the ARM site is higher than that reported for marine environments. The low å in marine

environments can be attributed to the dominance of large sea salt aerosols (Quinn et al., 1998).

The hemispheric backscatter fraction at the ARM site is similar in magnitude to those reported for Sagres and the marine sites. The mean hygroscopic growth factor of aerosols at the SGP CF is higher than that reported for Sagres, and is within the range of those reported for Linan, China. In contrast, it is lower than those reported for the marine environments, which implies that marine aerosols are more hygroscopic than continental aerosols. The suppression of hygroscopic growth at the continental sites (relative to marine sites) could be due to the influx of pollutants. For instance, Carrico et al. (2000) found that f(RH) was lower for polluted periods in comparison to laboratory measurements for pure deliquescent salts. In addition, hygroscopic growth of ambient sea-salt particles in the Pacific Northwest US was observed to be smaller than predicted from laboratory and modelling studies for pure NaCl particles, suggesting that organic compounds, possibly of anthropogenic origin, might cause the inhibition of particle growth (Pueschel et al., 1969).

Over a five-year period (1997–2001), annual means of total submicron aerosol concentration for particles with $D_p < 1\,\mu$m, particle concentration (N_p) for aerosols with $Dp < 10\,\mu$m, submicron light absorption coefficient and single scattering albedo at the SGP CF (at 550 nm) amount to $5306 \pm 392\,\mathrm{cm}^{-3}$, $654 \pm 290\,\mathrm{cm}^{-3}$, $2.0 \pm 0.7\,\mathrm{Mm}^{-1}$ and 0.94 ± 0.02, respectively, while those of submicron total scattering coefficient, hemispheric backscatter fraction, submicrometer scattering fraction at 550 nm and Ångström exponent (450 nm, 700 nm) are $36 \pm 2\,\mathrm{Mm}^{-1}$, 0.12 ± 0.01, 0.84 ± 0.03, 2.25 ± 0.09, respectively. The annual mean of f(RH) at the SGP CF from 1999 to 2001 amounts to 1.84 ± 0.10. Based on Koshmeider equation, annual mean visibility at the ARM site from 1997 to 2001 is 38 ± 2 km. The mean visibility at the ARM site is in agreement with that proposed for average continental aerosols (35 km) (Hess et al., 1998). While the mean value of b (0.12) at the ARM site is less than the global mean model value of b (0.15) assumed by Charlson et al.(1992) and Charlson and Heintzenberg (1995), the mean f(RH) at the site is close to their global f(RH) estimate

ACPD
3, 2353–2391, 2003

of 1.7.

Figure 6 presents the day-to-day variability of N_p, σ_a, R_{sp} and ω_0 at the SGP CF from 1997 to 2001 as well as the least square fit. The gaps in the plots imply missing or incomplete data. Although they exhibit a considerable year-to-year variability, in general, N_p and R_{sp} tend to increase by 97.8 cm^{-3} and 1.1% per year, respectively. While this short-term positive trend of N_p suggests an increase in total particle concentration at the ARM site, that of R_{sp} implies a rise in the proportion of smaller particles participating in scattering. σ_a shows an increase of 0.22 Mm^{-1} yr^{-1} while ω_0 declines by about 1% per year. Although a longer time series is necessary to achieve a more qualitative trend, the five-year inter-annual variations of aerosol optical properties at the SGP CF (shown in Fig. 6) are statistically significant at the 5% level (F-Test) and are indicative of an increased production of light-absorbing aerosols at the site. Biomass burning and fossil fuel combustion are the most important sources of light-absorbing aerosols. These sources are also linked to degradation of air quality and acid deposition (IPCC, 2001). Smoke aerosols produced by biomass burning contain a significant amount of black carbon particles (Crutzen and Andreae, 1990; Reid et al., 1998), which are important tracer of industrial pollution.

Kaufman et al. (1992) report an increase in ozone concentration due to biomass burning. We analyze ozone surface concentration data for the SGP CF from 1997 to 2001 and observe a rise in the annual mixing ration of O_3 at the site from about 35 ppbv in 1998 and 1999, to 36 and 45 ppbv in 2000 and 2001, respectively (see the first panel of Fig 7). In addition, we find that from 1997 to 2001, the annual precipitation at the ARM site has declined significantly from 3.11 mm d^{-1} to 1.53 mm d^{-1} (diminishing sharply at a rate of 0.38 mm dy^{-1} per year), while precipitable water vapor, relative humidity and cloud cover show a less pronounced negative tendency of -0.03 cm yr^{-1}, -0.4% yr^{-1} and -0.5% yr^{-1}, respectively (see Fig. 7). Due to the incomplete data set in 2000, we are not able to quantify the inter-annual variation of LWP.

The overall temporal decline in P_p, PWV, RH and A_c, which coincides with a rise in particle concentration, aerosol absorption coefficient and surface ozone, implies that

ACPD
3, 2353–2391, 2003

atmospheric conditions over the SGP are entering a drier phase. In particular, the marked deficit in precipitation at the ARM site in 2000 and 2001 is evident of drought (i.e. abnormally dry weather, which persist long enough to produce a severe hydrological imbalance). Drought is a natural and recurring phenomenon in Oklahoma's climate (occurring for example in 1988, 1998, 2000 and 2001). The year 2001 and the period June–August 2001 are reported as the 39th and fourth driest, respectively, in Oklahoma state since 1895 (Arndt, 2002).

The U.S. climate is mainly driven by the north Pacific. The very large El Nino of 1997 and 1998, which warmed Pacific Ocean waters, triggered unusual weather bringing rain and flooding to parts of the United States. Hong and Kalnay (2000) attributed the 1998 Oklahoma-Texas summer drought conditions to atmospheric conditions and sea surface temperature anomalies associated with waning El Nino and Southern Oscillation (ENSO) episode as well as soil moisture deficit. In summer 1999, faint traces of La Nina weather pattern emerged. La Nina resuscitated in the autumn of 1999 and intensified in 2000, continuing to 2001 (see http://www.cpc.noaa.gov/index.html). La Nina often brings warmer, dry weather to most of the United States. Consequently the drought conditions observed in 2000 and 2001 at the ARM site are a major consequence of La Nina. The drought of 1988 in the SGP region has been attributed to La Nina conditions (Atlas et al., 1993; Trenberth et al., 1988; Chen et al., 1998).

The production of biomass burning aerosols thrives in dry conditions, so that 2000 and 2001 are most favorable to smoke aerosols at the SGP. Absorption of solar radiation by smoke aerosols could lead to evaporation of cloud droplets or result in an increase in atmospheric stability (see Hansen et al., 1997; Ackerman et al., 2000; Lohmann and Feichter, 2001). While dry conditions enhance the concentration of aerosols near the surface, the decline in precipitation over the years at SGP CF could, in part, be facilitated by the effect of smoke aerosols to increase cloud condensation nuclei and cloud droplets number. This, in turn, will reduce cloud droplet size, coalescence and precipitation efficiency (see Rosenfeld, 1999).

ACPD
3, 2353–2391, 2003

4.2. Smoke and dust aerosols at the Southern Great Plains Central Facility

Most of the smoke haze observed at the ARM site originates from agricultural field burnings, local fire sources and oil refineries. However, smoke palls from remote forest fires have also been observed at the ARM site (Peppler et al., 2000). Figure 8 shows a NOAA AVHRR image as it captures smoke plumes (light blue) from numerous fires burning in Oklahoma, Kansas, Missouri and Arkansas on 28 March 2000 (21:49 UTC). Figure 9a presents aircraft-measured vertical profiles of light absorption coefficient on the afternoon (19:18–20:38 UTC) of 9 May 2000 (when no smoke was visible over the SGP) and on the afternoon (20:42–22:19 UTC) of 11 May 2000 (when intense smoke from the New Mexico forest fires was observed over SGP CF). Also presented on Fig. 9 are the mean vertical profiles of water vapor mixing ratio, relative humidity (retrieved from the ARM Raman Lidar), and air temperature (obtained from AERI) on the afternoon (20:00–21:00 UTC) of 9 and 11 May 2000. Lowest level values of r, RH and T_a are from SMOS and the 25/60 m Tower at the central facility. Up to 1 km above ground level (AGL), the light absorption coefficient recorded on the afternoon of 11 May is over 10 times that of 9 May. The difference in σ_a on the afternoon of these 2 days continues to be substantial up to about 2 km, indicating the considerable vertical extent of the smoke plume on 11 May 2000.

Contrary to the expectation of reduced r and RH (at lower levels) during drier and smoky periods as well as low wind speeds favorable to trapping aerosols close to the surface, we observe here that the relative humidity is higher in the lowest 1 km and the water vapor mixing ratio is higher up to 1.5 km on the afternoon of 11 May 2000. In the same vein, while the mean hourly surface wind speed from 19:00 to 22:00 UTC was only 5 ms^{-1} on 9 May 2000, it increased to 13 $m\,s^{-1}$ on 11 May 2000. These are strong indications that smoke aerosols are the major contributor to the observed variability of σ_a on 11 May 2000 at the SGP CF. In comparison with 9 May, the air is warmer throughout the boundary layer and free troposphere on the afternoon of 11 May. This could be due to the advection of a different air mass to the ARM site on 11 May. While

ACPD
3, 2353–2391, 2003

the flow was mainly northerly from 19:00 to 22:00 UTC on 9 May 2000, it was southerly on 11 May 2000.

Table 3 compares the inter-seasonal means of the optical properties of smoke-dominated haze ($D_p < 1\,\mu$m) with those for dusty and foggy conditions ($D_p < 10\,\mu$m) at the SGP CF from 1997 to 2001. Information about smoky, dusty and foggy conditions was obtained from the ARM Meta-data weather system. Dust plumes over the SGP CF originate mainly from the surrounding agricultural fields and are enhanced by gusty winds. There is a significant contribution to total absorption by dust particles, during strong dust outbreaks. ω_0 for smoke haze (0.91 ± 0.03) is much less than that of dust (0.96 ± 0.03) and fog (0.96 ± 0.01). One implication of this is that dust and fog generally scatter more radiation than smoke aerosols. Most foggy conditions at the SGP CF are recorded during winter. The single scattering albedo reported here for dust is within the same order of magnitude of those given by Dubovik et al. (2002) (i.e. $0.92 \leq \omega_0 \leq 0.99$) for desert dust. Hess et al. (1998) assumed $\omega_0 = 1.0$ for fog in their optical properties for aerosols and clouds (OPAC) dataset. As indicated by their mean Ångström exponent and hygroscopic growth factor (Table 3), smoke aerosols at the ARM site are smaller and more hygroscopic than dust. The aforementioned has significant consequence on the radiative effect of smoke and dust aerosols.

4.3. Net diabatic impact of aerosols

The net diabatic impact (NDI) of aerosols on the Earth atmosphere system can be deduced from ω_0, α and β, where β is the fraction of radiation scattered upwards by aerosols and α is the albedo of the underlying surface. The net aerosol impact is a warming if

$$\mathrm{NDI} = \omega_0 - \{2\alpha/[\beta(1-\alpha)^2 + 2\alpha]\} < 0 \quad (7)$$

and cooling otherwise (Hegg et al., 1996). We obtain α from measurements of upwelling and downwelling shortwave radiation, and compute β at 550 nm from nephelometer backscattering measurements according to Sheridan and Ogren (1999). Sea-

sonal values for β range from 0.25 to 0.30 (see Table 4). This range of values for β is in agreement with those reported by Charlson et al. (1992), Chylek and Wong (1995), and Hobbs et al. (1997). Figure 10 presents NDI for aerosols at the SGP. Since NDI (which ranges from 0.17 to 0.28 for all examined cases) is positive in all seasons, it follows that smoke- and dust-dominated haze, as well as all aerosols combined, produce a net diabatic cooling at the ARM site. This is quite different from the effect of Arctic haze, which produces a net warming in winter (Ackerman et al., 1986). In June, however, Arctic aerosols produce a net cooling in the atmosphere (Hegg et al., 1996). In general, the cooling produced by dust at the ARM site exceeds that of smoke, while the annual NDI for all aerosols (0.20) at the SGP lies approximately halfway between that for smoke and dust. The net diabatic cooling of aerosols at the ARM site is most pronounced in the spring owing to the relatively high single scattering albedo during this season.

4.4. On the direct radiative forcing of aerosols

Based on the box-model of direct radiative forcing ΔF_R of aerosols proposed by Charlson et al. (1992) and extended by Chylek and Wong (1995), Iziomon and Lohmann (2003) presented seasonal estimates of ΔF_R for smoke-dominated haze at the SGP CF. Here we compare seasonal ΔF_R for smoke, dust and all aerosols combined at the ARM site. The extinction optical depth τ_{ext} is given by the sum of the optical depth for light scattering τ_{sc} (where $\tau_{sc} = \omega_0 \tau_{ext}$) and the optical depth for light absorption τ_a. τ_{ext} at 550 nm is computed from nephelometer measurements according to Bergin et al. (1996, 2000). Table 4 presents seasonal estimates of β, τ_{sc}, τ_a and ΔF_R at the SGP CF (at 550 nm) for smoke and dust dominated haze as well as all aerosols combined at the SGP CF. Direct radiative forcing is particularly sensitive to the single scattering albedo.

In absolute terms, the inter-seasonal mean of ΔF_R for dust-dominated haze ($-1.3\,W\,m^{-2}$) at the SGP CF is slightly less than that for smoke-dominated haze ($-1.4\,W\,m^{-2}$). The high negative ΔF_R for smoke dominated haze in spring relative

ACPD
3, 2353–2391, 2003

to other seasons is mainly attributable to aerosol aging, higher extinction coefficient and single scattering albedo of smoke aerosols. In general, the total direct radiative forcing of all aerosols at the SGP exhibits an inter-seasonal mean of $-1.5 \pm 0.8\,\mathrm{Wm}^{-2}$, with a maximum in the summer. Among others, the low solar elevation in winter partially accounts for the relatively low ΔF_R observed in the season. The inter-seasonal estimate of ΔF_R for the ARM site agrees with the range (-0.07 to $-1.24\,\mathrm{Wm}^{-2}$) of the IPCC global estimate of total direct radiative forcing from industrial aerosols (IPCC, 2001). Since the number of available studies is still very limited, IPCC has not yet assigned a best estimate for the global ΔF_R of dust aerosols, but proposes a tentative range of -0.6 to $+0.4\,\mathrm{Wm}^{-2}$ (IPCC 2001).

5. Summary and conclusions

Although tropospheric aerosols are of significant importance to climate change and contribute substantially to the radiative forcing of the Earth's climate, the understanding of their climatic influence is compounded by their variable concentrations. The continuous measurements of aerosol and meteorological variables by the ARM Program are capable of helping us to improve our understanding of feedback mechanisms, radiative and cloud effects associated with aerosols.

It is noteworthy that the highest mean values of submicron light absorption coefficient, light scattering coefficient and OPC-measured particle concentration are recorded in the summer at the site. In addition, the estimated direct radiative forcing of aerosols at the ARM site ranges from $-0.7\,\mathrm{W\,m}^{-2}$ (in winter) to $-2.4\,\mathrm{W\,m}^{-2}$ (in summer), with an inter-seasonal mean value of $-1.5 \pm 0.8\,\mathrm{W\,m}^{-2}$. The foregoing shows that relative to winter, the atmosphere over the SGP in the summer season is less pristine. Aerosol pollution in the summer could be due to a number of factors including agricultural field burning activities and smoke plumes from remote forest fires, wind-enhanced dust episodes, as well as emissions from automobiles, oil refineries and power plants. In particular biomass burning activities are more frequent at the ARM

ACPD
3, 2353–2391, 2003

site in the summer season (and late spring) (Iziomon and Lohmann, 2003). We observe from the ARM data that σ_s and R_{sp} decrease with wavelength while b increases with it. In contrast to the effect of Arctic haze, which produces a net warming in winter (see Ackerman et al. 1986; Hegg et al., 1996), aerosols at the SGP CF produce a net diabatic cooling in all seasons.

The inter-seasonal mean of ω_0 for smoke haze (0.91 ± 0.03) at the ARM site is much less than that for dust (0.96 ± 0.03). This indicates that dust aerosols scatter more radiation than does smoke aerosols. The Ångström exponent at the ARM site is higher than that reported for marine environments. The low å in marine environments can be attributed to the dominance of large sea salt aerosols (Horvath, 1993; Quinn et al., 1998). Furthermore, the mean hygroscopic growth factor of aerosols at the SGP CF is lower than those reported for the marine environments. The suppression of hygroscopic growth at the continental sites (relative to marine sites) could be due to the influx of pollutants.

The decline in precipitation, column integrated water vapor and cloud fraction particularly for 2000 and 2001 at the ARM site is associated with drought. The observed inter-annual variability of σ_a could be indirectly related with the increasingly dry surface conditions at the site. While we acknowledge that less precipitation implies less aerosol scavenging and that atmospheric stability due to an anticyclonic air mass during dry conditions could hamper cloud formation, we also do not rule out the possibility of the aerosol semi-direct effect for the observed downward trend in A_c. Aerosol chemical analysis at the SGP are not presented here, since the measurement of aerosol chemical properties has only commenced recently at the SGP CF, but shall be the subject of a future study.

Acknowledgement. The data used for this study were obtained from the Atmospheric Radiation Measurement (ARM) Program sponsored by the U.S. Department of Energy, Environmental Sciences Division. The authors thank the awarding agency as well as ARM staffs for operating the ARM sites and maintaining the database, the aerosol group at NOAA Climate Monitoring and Diagnostics Laboratory for operating the Aerosol Observing System and the Dalhousie

University Killam Trust for support.

References

Ackerman, T. P., Stenback, J. M., and Valero, F .P. J.: The importance of Arctic haze for the energy budget of the Arctic, in Artic Air Pollution, edited by B. Stonehouse, 151–158, Cambridge Univ. Press, New York, 1986.

Ackerman, S. A. and Chung, H.: Radiative effects of airborne dust on regional energy budgets at the top of the atmosphere, J. Appl. Meteor., 31, 223–233, 1992.

Ackerman, A. S., Toon, O. B., Stevens, D. E., Heymsfield, A. J., Ramanathan, V., and Welton, E. J.: Reduction of tropical cloudiness by soot, Science, 288, 1042–1047, 2000.

Anderson, B. E., Grant, W. B., Gregory, G. L., Browell, E. V., Collins Jr., J. E., Sachse, D. W., Bagwell, D. R., Hudgins, C. H., Blake, D. R., and Blake, N. J.: Aerosols from biomass burning over the tropical South Atlantic region: Distributions and impacts, J. Geophys. Res., 101, 24 117–24 137, 1996.

Andreae, M. O., Atlas, E., Cachier, H., Cofer, W. R., Harris, G. W., Helas, G., Koppman, R., Lacaux, J.P, and Ward, D. E.: Trace gas and aerosol emissions from savanna fires, in Biomass Burning and Global Change, edited by J. S. Levine, 278–295, MIT Press, Cambridge, Mass., 1996.

Andreae, M. O., Artaxo, P., Fischer, H., Freitas, S. R., Grégoire, J.M, Hansel, A., Hoor, P., Kormann, R., Krejci, R., Lange, L., Lelieveld, J., Lindinger, W., Longo, L., Peters, W., De Reus, M., Scheeren, B., Silva Dias, MA. F., Ström, J., Van Velthoven, P. F. J., and Williams, J.: Transport of biomass burning smoke to the upper troposphere by deep convection in the equatorial region, J. Geophys. Res., 28, 951–954, 2001.

Arndt, D. S.: The Oklahoma drought of 2001–2002, Oklahoma Climatological Survey Climate Event Summary, ES 2002-02, 31, 2002.

Atlas, R., Wolfson, N., and Terry, J.: The effects of SST and soil moisture anomalies on GLA model simulations of the 1988 US summer drought, J. Clim., 6, 2034–2048, 1993.

Baumgardner, D., Raga, G. B., Kok, G., Ogren, J., Rosas, I. Baez, A., and Novakov, T.: On the evolution of aerosol properties at a mountain site above Mexico City, J. Geophys. Res., 105, 22 243–22 253, 2000.

Bergin, M. H., Ogren, J. A., Halthore, R. N., Nemesure, S., and Schwartz, S. E.: Aerosol op-

tical depth estimates based on Nephelometer measurements at the Atmospheric Radiation Measurement Southern Great Plains Site, Proceedings of the Sixth Atmospheric Radiation Measurement Science Team Meeting, USA, 27–30, 1996.
Bergin, M. H., Halthore, R. S., Schwartz, S. E., Ogren, J. A., and Nemesure, S.: Comparison of Aerosol Column Properties Based on Nephelometer and Radiometer Measurements at the SGP ARM Site, J. Geophys. Res., 105, 6807–6816, 2000.
Bergin, M. H., Cass, G. R., Xu, J., Fang, C., Zeng, L. M., Yu, T., Salmon, L. G., Kiang, C. S., Tang, X. Y., Zhang, Y. H., and Chameides, W. L.: Aerosol Radiative, Physical, and Chemical Properties in Beijing During June, 1999, J. Geophys. Res., 106, 17 969–17 980, 2001.
Bond, T. C., Anderson, T. L., and Campbell, D.: Calibration and intercomparison of filter-based measurements of visible light absorption by aerosols, Aerosol Sci. Technol., 30, 582–600, 1999.
Bréon, F-M., Tanré, D., and Generoso, S.: Aerosol effect on cloud droplet size monitored from satellite, Science, 295, 834–838, 2002.
Carrico, C. M., Rood, M. J., and Ogren, J. A.: Aerosol light scattering properties at Cape Grim, Tasmania, during the first aerosol characterization experiment (ACE 1), J. Geophys. Res., 103, 16 565–16 574, 1998.
Carrico, C. M., Rood, M. J., Ogren, J. A., Neususess, C., Wiedensohler, A., and Heintzenberg, J.: Aerosol optical properties at Sagres, Portugal during ACE-2, Tellus, 52B, 694–715, 2000.
Charlson, R. J., Schwartz, S. E., Hales, J. M., Cess, R. D., Coakley, Jr, J. A., Hansen, J. E., and Hofmann, D. J.: Climate forcing by anthropogenic aerosols, Science, 255, 423–430, 1992.
Charlson, R. J. and Heintzenberg, J.: Introduction, in Aerosol Forcing of Climate, edited by J. Heintzenberg and R. J. Charlson, John Wiley, New York, 1–10, 1995.
Chen, P. and Newman, M.: Rossby wave propagation and the rapid development of upper level anomalous anticyclones during the 1988 US drought, J. Clim., 11, 2491–2504, 1998.
Chylek, P. and Wong, J.: Effect of absorbing aerosols on global radiation budget, Geophys. Res. Lett., 22, 929–931, 1995.
Crutzen, P. J. and Andreae, M. O.: Biomass burning in the tropics: impact on atmospheric chemistry and biogeochemical cycles, Science, 250, 1669–1678, 1990.
Dubovik, O., Holben, B., Eck, T. F., Smirnov, A., Kaufman, Y. J., King, M. D., Tanre, D., and Slutsker, I.: Variability of absorption and optical properties of key aerosol types observed in worldwide locations, J. Atmos. Sci., 59, 590–608, 2002.
Eck, T. F. Holben B. N., Dubovik O., Smirnov A., Slutsker I., Lobert J. M., and Ramanathan, V.:

ACPD
3, 2353–2391, 2003

Column integrated aerosol optical properties over Maldives during NE Monsoon for 1998-2000, J. Geophys. Res., 106, 28 555–28 566, 2001.
Griffin, G. W.: Relationships between the prevailing visibility, nephelometer scattering coefficient, and sunphotometer turbidity coefficient, Atmos. Environ., 14, 577–584, 1980.
Hansen, J., Sato, M., and Ruedy, R.: Radiative forcing and climate response, J. Geophys. Res., 102, 6831–6864, 1997.
Haywood, J. M., Ramaswamy, V., and Soden, B. J.: Tropospheric aerosol climate forcing in clear-sky satellite observations over the oceans, Science, 283, 1299–1303, 1999.
Hegg, D. A., Hobbs, P. V., Gasso, S., Nance, J. D., Rangno, A. L.: Aerosol measurements in the Arctic relevant to direct and indirect radiative forcing, J. Geophys. Res., 101, 23 349–23 363, 1996.
Hess, M., Koepke, P., and Schult, I.: Optical properties of aerosols and clouds: The software package OPAC, Bull. Amer. Meteorol. Soc., 79, 831–844, 1998.
Husar, R. B., Poll, D. E., Holloway, J. M., Wilson, W. E., and Ellestad, T. G.: Trends of eastern U.S. haziness since 1948, Prepint Volume: Fourth symposium on turbulence, American Meteorology Society, Boston, MA, 249–256, 1979.
Hobbs, P. V., Reid, J. S., Kotchenruther, R. A., Ferek, R. J., and Weiss, R.: Direct Radiative Forcing by Smoke from Biomass Burning, Science, 275, 1777–1778, 1997.
Hong, S-Y. and Kalnay, E.: Role of sea surface temperature and soil-moisture feedback in the 1998 Oklahoma-Texas drought, Nature, 408, 842–844, 2000.
Horvath, H.: Atmospheric light absorption-a review, Atmos. Environ. 27A, 293–317, 1993.
Intergovernmental Panel on Climate Change (IPCC): Climate Change 2001: The scientific basis, edited by J. T. Houghton et al., Cambridge University Press, New York, 2001.
Iziomon, M. G. and Lohmann, U.: Optical and meteorological properties of smoke-dominated haze at the ARM Southern Great Plains central facility, Geophys. Res. Lett. 30, 1123, doi:10.1029/2002GLO16606, 2003.
Kaufman, Y. J., Setzer, A., Ward, D., Tanre, D., Holben, B. N., Menzel, P., Pereira, M. C., and Rasmussen, R.: Biomass burning airborne and spaceborne experiment in the Amazonas (BASE-A), J. Geophys. Res. 97, 14 581–14 599, 1992.
Kaufman, Y. J., Hobbs, P. V., Kirchhoff, V. W. J. H., Artaxo, P., Remer, L. A., Holben, B. N., King, M. D., Ward, D. E., Prins, E. M., Longo, K. M., Mattos, L. F., Nobre, C. A., Spinhirne, J. D., Ji, Q., Thompson, A. M., Gleason, J. F., Christopher, S. A., and Tsay, S.-C.: Smoke, Clouds, and Radiation-Brazil (SCAR-B) experiment, J. Geophys. Res., 103, 31 783–31 808, 1998.

ACPD
3, 2353–2391, 2003

Koshmeider, H.: Theorie der horizontale Sichtweite, Betrag. Atm. Physik., 12, 33–55, 1926.
Kotchenruther, R. A., Hobbs, P. V., and Hegg, D. A.: Humidification factors for atmospheric aerosols off the mid-Atlantic coast of the United States, J. Geophys. Res., 104, 2239–2251, 1999.
Leaitch, W. R., Isaac, G. A., Strapp, J. W., Banic, C. M., and Wiebe, H. A.: The relationship between cloud droplet number concentrations and anthropogenic pollution: observations and climatic implications, J. Geophys. Res., 97, 2463–2474, 1992.
Le Canut, P., Andreae, M. O., Haris, G. W., Weinhold, F. G., and Zenker, T.: Airborne studies of emissions from savanna fires in southern Africa. 1, Aerosol emissions measured with a laser particle counter, J. Geophys. Res., 101, 23 615–23 630, 1996.
Lelieveld, J., Crutzen, P. J., Ramanathan, V., Andreae, M. O., Brenninkmeijer, C. A. M., Campos, T., Cass, G. R., Dickerson, R. R. Fischer, H., De Gouw, J. A., Hansel, A., Jefferson, A., Kley, D., De Laat, A. T. J., Lal, S., Lawrence, M. G., Lobert, J. M., Mayol-Bracero, L., Mitra, A. P., Novakov, T., Oltmans, S. J., Prather, K. A., Reiner, T., Rodhe, H., Scheeren, H. A., Sikka, D., and Williams, J.: The Indian Ocean Experiment: widespread air pollution from south and south east Asia, Science, 291, 1031–1036, 2001.
Lohmann, U., Feichter, J., Penner, J., and Leaitch, R.: Indirect effect of sulfate and carbonaceous aerosols: A mechanistic treatment, J. Geophys. Res. 105, 12 193–12 206, 2000.
Lohmann, U. and Feichter, J.: Can the direct and semi-direct aerosol effect compete with the indirect effect on a global scale?, Geophys. Res. Lett., 28, 159–161, 2001.
Nakajima, T., Higurashi, A., Kawamoto, K., and Penner, J. E.: A possible correlation between satellite-derived cloud and aerosol microphysical parameters, Geophys. Res. Lett., 28, 1171–1174.
Ozkaynak, H. A., Schatz, D., Thurston, G. D., Isaacs, R. G., and Husar, R. B.: Relationships between aerosol extinction coefficient derived from airport visual range observations and alternative measure of airborne particle mass, J. Air Pollution Contr. Assoc., 35, 1176–1185, 1985.
Penner, J. E., Charlson, R. J., Hales, J. M., Laulainen, N. S., Leifer, R. Novakov, T., Ogren, J., Radke, L. F., Schwartz, S. E., and Travis, L.: Quantifying and minimizing uncertainty of climate forcing by anthropogenic aerosols, Bull. Am. Meteorol. Soc., 75, 375–400, 1994.
Peppler, R. A., Bahrmann, C. P, Barnard, J. C., Campbell, J. R., Cheng, M.-D., Ferrare, R. A., Halthore, R. N., Heilman, L. A., Hlavka, D. L., Laulainen, N. S., Lin, C.-J., Ogren, J. A., Poellot, M. R., Remer, L. A., Sassen, K., Spinhirne, J. D., Splitt, M. E., and Turner, D. D.:

ARM Southern Great Plains site observations of the smoke pall associated with the 1998 Central American fires, Bull. Amer. Met. Soc., 81, 2563–2591, 2000.
Pueschel, R. F., Charlson, R. J., and Ahlquist, N. C.: On the anomalous deliquescence of sea-spray aerosols, J. Appl. Met., 8, 995–998, 1969.
Platnick, S., Durkee, P. A., Nielsen, K., Taylor, J. P., Tsay, S-C., King, M. D., Ferek, R. J., Hobbs, P. V., and Rottman, J. W.: The role of background cloud microphysics in the radiative formation of shiptracks, J. Atmos. Sci., 57, 2607–2624, 2000.
Prospero, J.: Long-term measurements of the transport of African mineral dust to the Southeastern United States: Implications for regional air quality, J. Geophys. Res., 104, 15 917–15 927, 1999.
Quinn, P. K., Coffman, D. J., Kapustin, V. N., Bates, T. S.: Aerosol optical properties in the marine boundary layer during the first aerosol characterization experiment (ACE1) and the underlying chemical and physical aerosol properties, J. Geophys. Res., 103, 16 547–16 563, 1998.
Quinn, P. K., Bates, T. S., Coffman, D. J., Miller, T. L., Johnson, J. E., Covert, D. S., Putaud, J. P., Neususs, C., and Novakov, T.: A comparison of aerosol chemical and optical properties from the first and second aerosol characterization experiments, Tellus 52B, 239–257, 2000.
Radke, L. F., Coakley, Jr. J. A., and King, M.: Direct and remote sensing observations of the effects of ships on clouds, Science, 246, 1146–1149, 1989.
Reid, J. S, Hobbs, P. V., Ferek, R. J., Blake, D. R., Martins, J. V., Dunlap, M. R., and Liousse, C.: Physical, chemical and optical properties of regional hazes dominated by smoke in Brazil, J. Geophys. Res., 103, 32 059 –32 080, 1998.
Remer, L. A., Kaufman, Y. J., Holben, B. N., Thompson, A. M., and McNamara, D.: Biomass burning aerosol size distribution and modeled optical properties, J. Geophys. Res., 103, 31 879–31 891, 1998.
Rosenfeld, D.: TRMM observed first direct evidence of smoke from forest fires inhibiting rainfall, Geophys. Res. Lett., 26, 3105–3108, 1999.
Ross, J. L., Hobbs, P. V., and Holben, B.: Radiative characteristics of regional hazes dominated by smoke from biomass burning in Brazil: Closure tests and direct radiative forcing, J. Geophys. Res. 103, 31 925–31 941, 1998.
Scheff, P. A. and Valiozis, C.: Characterization and source identification of respirable particulate matter in Athens, Greece, Atmos. Environ., 24A, 203–211, 1990.
Schichtel, B. A., Husar, R. D., Falke, S. R., and Wilson W. E.: Haze trends over the United

States, 1980–1995, Atmos. Environ., 35, 5205–5210, 2001.
Sheridan, P. J. and Ogren, J. A.: Observations of the vertical and regional variability of aerosol optical properties over central and eastern North America, J. Geophys. Res., 104, 16 793–16 805, 1999.
Sheridan, P. J., Delene, D. J., and Ogren, J. A.: Four years of continuous aerosol measurement from the Department of Energy's Atmospheric radiation measurement program southern great plains cloud and radiation testbed site, J. Geophys. Res., 106, 20 735–20 747, 2001.
Tanre, D., Breon, F. M., Deuze, J. L., Herman, M., Goloub, P., Nadal, F., and Marchand, A.: Global observation of anthropogenic aerosols from satellite, Geophys. Res. Lett., 28, 4555–4558, 2001.
Trenberth, K. E., Branstator, G. W., and Arkin, P. A.: Origins of the 1988 North American drought, Science, 242, 1640–1645, 1988.
Twomey, S. A.: Aerosols, clouds and radiation, Atmos. Environ., 25A, 2435–2442, 1991.
Vasilyev, O. B., Levya Contreras, A., Muhlia Velazquez, A., Peralta y Fabi, R. et al.: Spectral optical properties of the polluted atmosphere of Mexico City (spring summer 1992), J. Geophys. Res., 100, 26 027–26 044, 1995.
Weber, R. J., Marti, J. J., McMurry, M. J., Eisele, F. J., Tanner, D. J., and Jefferson, A.: Measurements of new particle formation and ultrafine particle growth rates at a clean continental site, J. Geophys. Res., 102, 4375–4385, 1997.
Xu, J., Bergin, M. H., Yu, X., Liu, G., Zhao, J., Carrico, C. M., and Baumann, K.: Measurement of aerosol chemical, physical and radiative properties in the Yangtze delta region of China, Atmos. Environ. 36, 161–173, 2002.
Weingartner, E., Nyeki, S., and Baltensperger, U.: Seasonal and diurnal variation of aerosol size distributions (10<D<750 nm) at a high-alpine site (Jungfraujoch 3580 m a.s.l.), J. Geophys. Res., 104, 26 809–26 820, 1999.

Table 1. Seasonal median of daily total number concentration of condensation particles Na, OPC measured particle concentration N_p, light absorption coefficient σ_a, light scattering coefficient σ_s, hemispheric backscatter fraction b, submicrometer scattering fraction R_{sp} single scattering coefficient ω_0 and Ångström exponent å at the SGP CF 1997–2001

Variables	λ (nm)	Winter	Spring	Summer	Autumn	All seasons
N_a (cm^{-3})	780	4737	5578	4875	5007	5065
N_p (cm^{-3})	633	443	535	884	528	551
σ_a (Mm^{-1})	~550	1.36	1.20	2.21	1.76	1.62
	450	40.6	44.6	50.7	38.6	43.0
σ_s (Mm^{-1})	550	27.5	29.9	33.6	25.1	28.9
	700	15.9	17.0	19.7	14.1	16.9
	450	0.10	0.11	0.10	0.11	0.11
b	550	0.11	0.13	0.12	0.13	0.12
	700	0.16	0.17	0.16	0.18	0.17
	450	0.92	0.88	0.87	0.90	0.89
R_{sp}	550	0.90	0.84	0.82	0.86	0.85
	700	0.85	0.78	0.74	0.80	0.79
ω_0	550	0.95	0.95	0.93	0.93	0.94
	450, 550	1.90	2.01	1.98	2.02	1.98
å	450, 700	2.06	2.17	2.15	2.19	2.15
	550, 700	2.22	2.30	2.28	2.32	2.28

ACPD
3, 2353–2391, 2003

Table 2. Mean aerosol light absorbing coefficient σ_a, total light scattering coefficient σ_s, hemispheric backscattering fraction b, Ångström exponent å, single scattering albedo ω_0 and hygroscopic growth factor f(RH) (at 550 nm) for June and July at the ARM site with those measured over the same period (except for Linan, China) during some major aerosol field campaigns (see text for more details)

Air mass origin	Location	σ_a (Mm^{-1})	σ_s (Mm^{-1})	b	å	ω_0	f(RH)
Continental	SGP CF[a]	2.8±1.2	41±6	0.11	2.1±0.1	0.94±0.2	1.8±0.2
	Sagres[b]	--	43±19	0.12±0.02	2.5±0.1	--	1.5±0.1
	Linan[c]	23±14	353±202	--	--	0.93±0.04	1.7-2.0
	Beijing[d]	83±40	488±370	--	--	0.81±0.08	--
Marine	Cape Grim[e]	--	5.4±3.0	0.12±0.03	1.4±0.5	--	2.4±0.4
	ACE 1[fg]	0.2±0.3	4.1±2.8	0.11±0.02	1.2±0.3	0.99±0.01	--
	Atlantic[gh]	0.4± 0.2	4.6±3.4	--	0.2±0.2	0.98±0.01	2.3±0.2
	Polar[g]	0.4±0.3	4.0±1.0	--	0.3±0.3	0.97±0.02	--

(a) present study; (b) Carrico et al., 2000; (c) Xu et al., (2002); (d) Bergin et al., (2001); (e) Carrico et al., (1998); (f) Quinn et al., (1998); (g) Quinn *et al*. (2000); (h) Kotchenrurther et al. (1999)

ACPD
3, 2353–2391, 2003

Table 3. Inter-seasonal mean of hourly single scattering albedo ω_0 (at 550 nm), hemispheric backscatter fraction b (at 550 nm), Ångström exponent å (450 nm, 750 nm), and hygroscopic growth factor f(RH) (at 550 nm) for smoky, dusty and foggy conditions at ARM SGP CF

Constituent	ω_0	b	å	f(RH)
Smoke	0.91±0.03	0.14±0.02	2.0±0.1	1.6±0.2
Dust	0.96±0.03	0.13±0.02	1.6±0.2	1.4±0.6
Fog	0.96±0.01	0.11±0.01	2.0±0.1	1.9±0.2

ACPD
3, 2353–2391, 2003

Table 4. Seasonal estimates of aerosol upscatter fraction β, optical depth for light scattering (τ_{sc}), optical depth for light absorption τ_a and aerosol direct radiative forcing ΔF_R (W m^{-2}) at 550 nm at the SGP CF

Variables	Aerosol Type	Season				All Seasons
		Winter	Spring	Summer	Autumn	
β	Smoke	0.28	0.25	0.28	0.30	0.28±0.02
	Dust	0.27	0.28	0.25	0.27	0.27±0.01
	All aerosols	0.26	0.27	0.26	0.27	0.27±0.01
τ_{sc}	Smoke	0.032	0.141	0.071	0.032	0.069±0.05
	Dust	0.044	0.0485	0.029	0.085	0.052 ±0.02
	All aerosols	0.066	0.068	0.078	0.057	0.067 ±0.01
τ_a	Smoke	0.003	0.009	0.009	0.004	0.006±0.003
	Dust	0.001	0.0005	0.002	0.006	0.002±0.002
	All aerosols	0.004	0.004	0.006	0.005	0.005±0.001
ΔF_R (W m^{-2})	Smoke	-0.25	-3.14	-1.74	-0.52	-1.4±1.3
	Dust	-0.65	-1.79	-0.90	-1.72	-1.3±0.6
	All aerosols	-0.67	-1.82	-2.44	-1.04	-1.5±0.8

ACPD
3, 2353–2391, 2003

Fig. 1. ARM map showing the Southern Great Plains Region and surrounding locations.

ACPD
3, 2353–2391, 2003

Characteristics, impacts and direct radiative forcing of aerosols

M. G. Iziomon and U. Lohmann

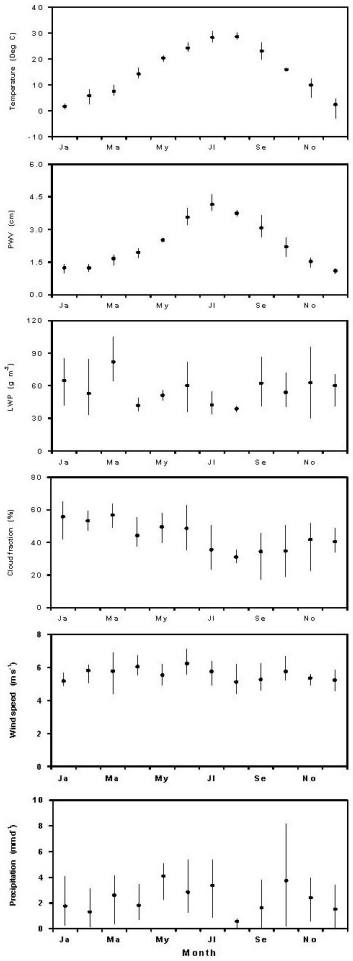

Fig. 2. Surface meteorological variables at the ARM SGP CF.

ACPD

3, 2353–2391, 2003

Characteristics, impacts and direct radiative forcing of aerosols

M. G. Iziomon and U. Lohmann

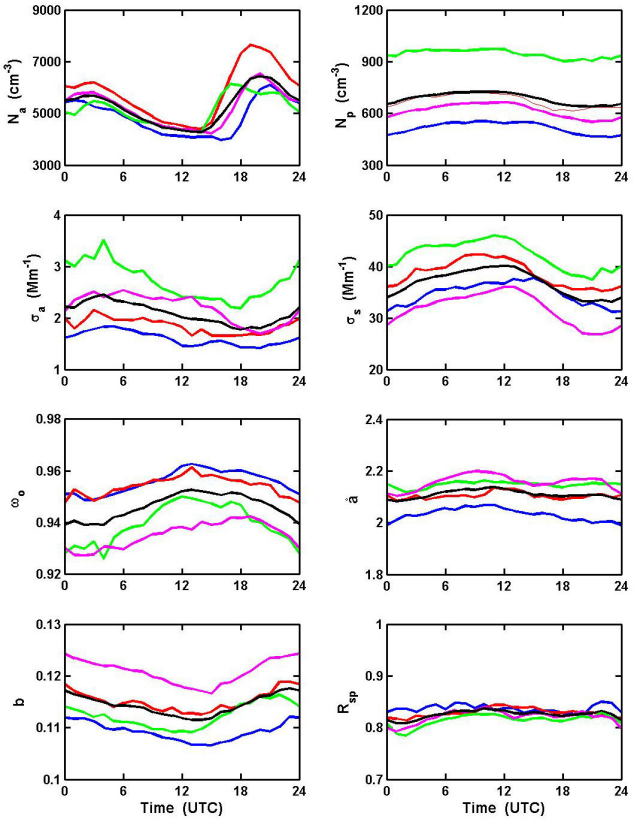

Fig. 3. Mean diurnal variation of total number concentration of condensation particles N_a, OPC-measured particle concentration N_p, light absorption coefficient σ_a, light scattering coefficient σ_s, single scattering coefficient ω_0, Ångström exponent å, hemispheric backscatter fraction b, and submicrometer scattering fraction R_{sp} in winter (blue), spring (red), summer (green), autumn (magenta) and during all seasons (black line) at the ARM SGP CF.

ACPD
3, 2353–2391, 2003

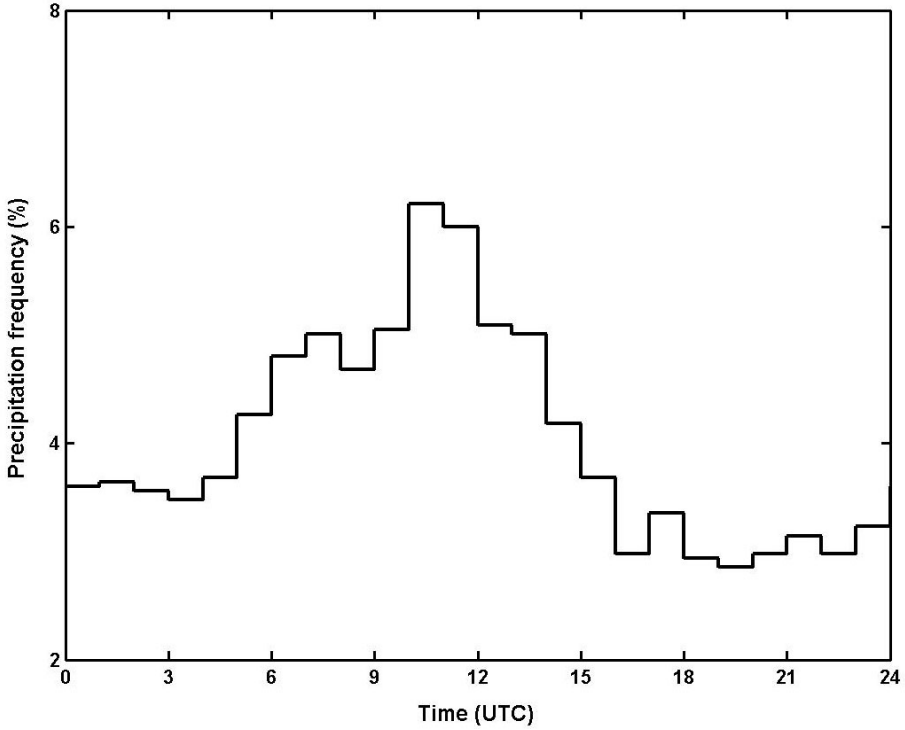

Fig. 4. Frequency distribution of hourly precipitation at the ARM Southern Great Plains central facility 1997–2001.

ACPD
3, 2353–2391, 2003

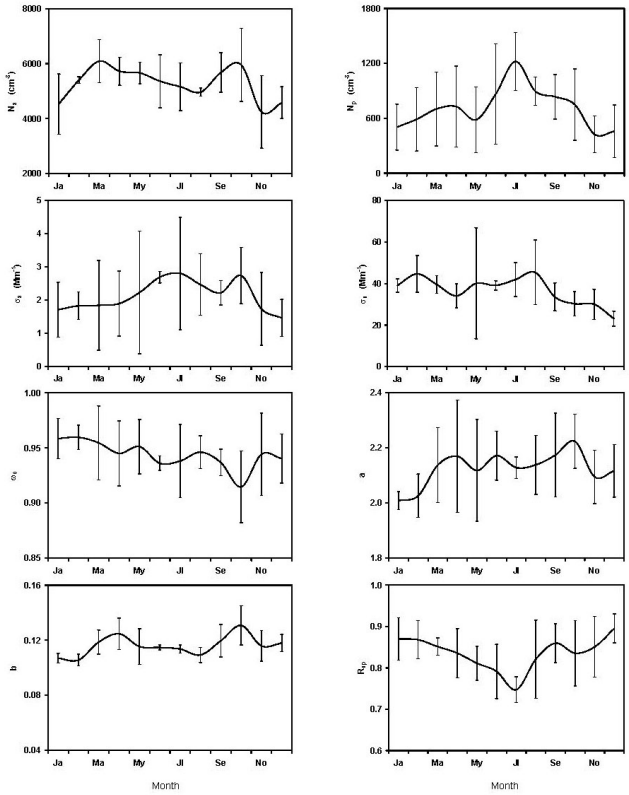

Fig. 5. Monthly mean and standard deviation of submicron total particle concentration N_s, OPC-measured particle concentration N_p, submicron light absorption coefficient σ_a, light scattering coefficient σ_s, single scattering coefficient ω_0, Angstrom exponent a, hemispheric backscatter fraction b and submicrometer scattering fraction R_{sp}.

ACPD
3, 2353–2391, 2003

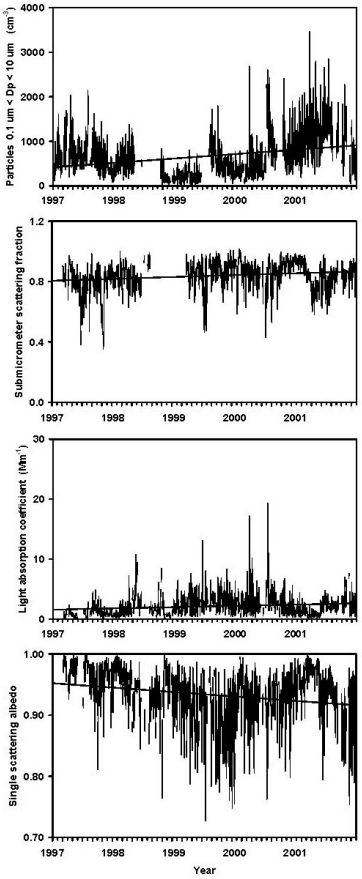

Fig. 6. Day to day variability of OPC-measured particle concentration, submicrometer scattering fraction, light absorption coefficient and single scattering albedo at the ARM site.

ACPD

3, 2353–2391, 2003

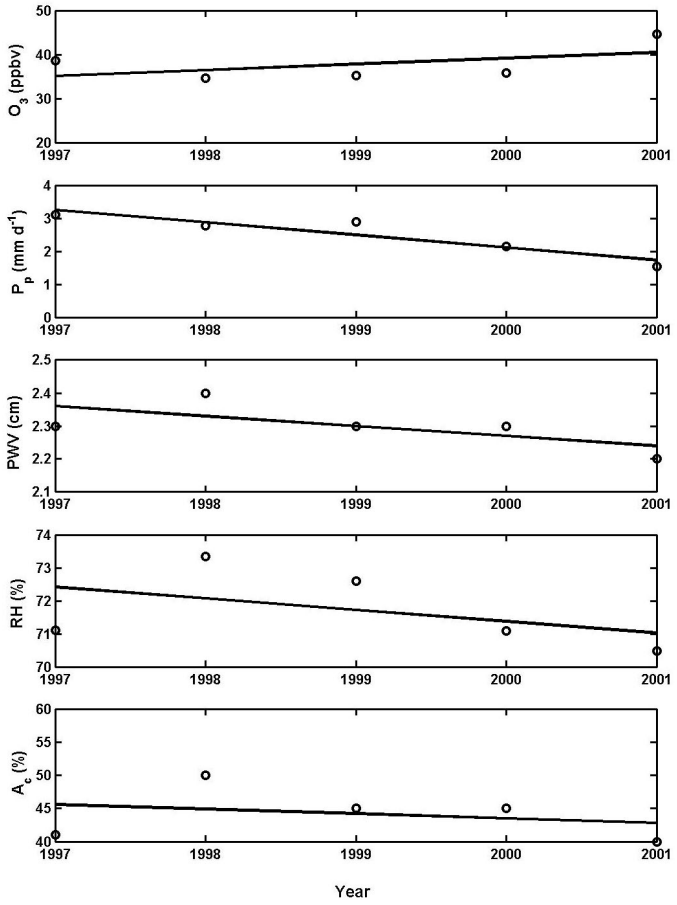

Fig. 7. Least square fit of annual mean ozone (O_3) mixing ratio, precipitation P_p, precipitable water vapor PWV, relative humidity RH and cloud cover A_c at SGP CF from 1997 to 2001.

ACPD
3, 2353–2391, 2003

Characteristics, impacts and direct radiative forcing of aerosols

M. G. Iziomon and U. Lohmann

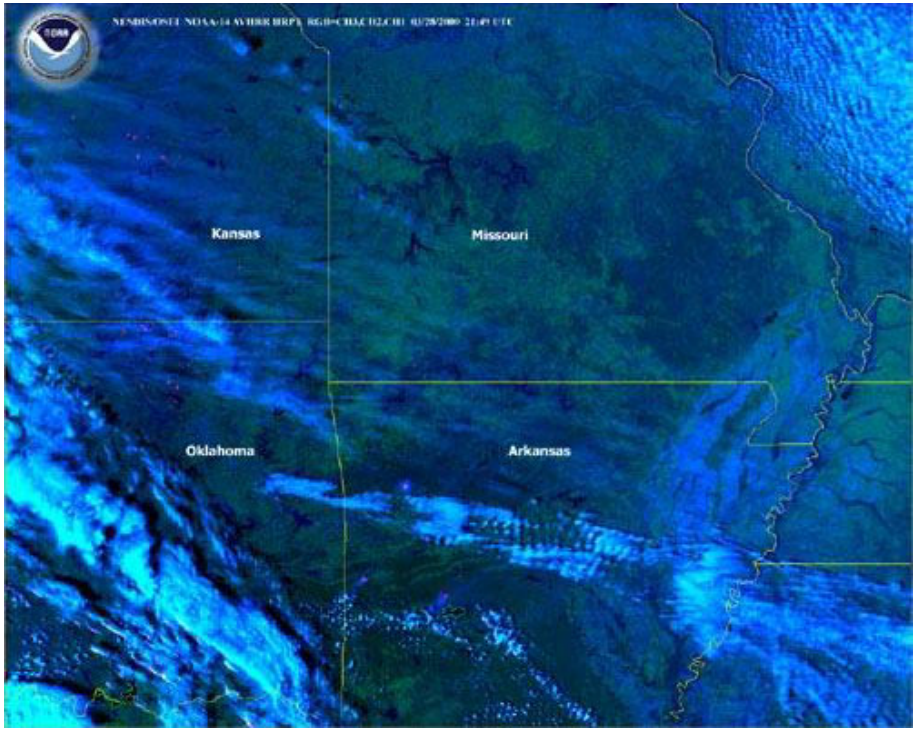

Fig. 8. NOAA AVHRR images showing smoke plumes (light blue) from numerous fires burning in Oklahoma, Kansas, Missouri and Arkansas on 28 March 2000 (21:49 UTC).

ACPD
3, 2353–2391, 2003

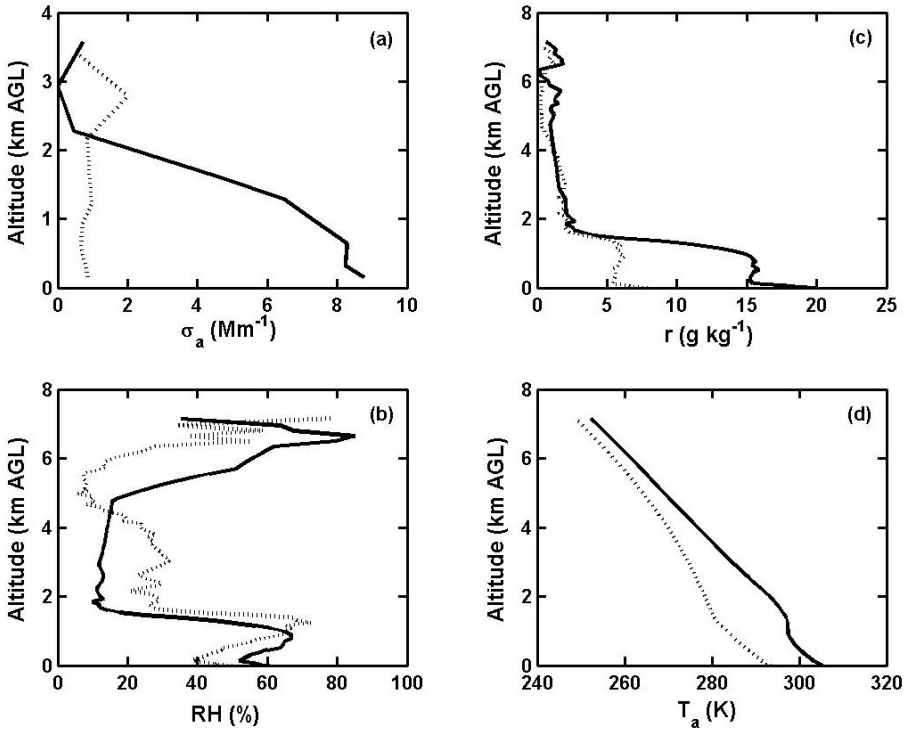

Fig. 9. Vertical profile of **(a)** light absorption coefficient σ_a, **(b)** water vapor mixing ratio r, **(c)** relative humidity (RH) and **(d)** air temperature T_a before (9 May: dotted line) and during (11 May: solid line) a smoke event at the SGP CF (see Text for details).

ACPD
3, 2353–2391, 2003

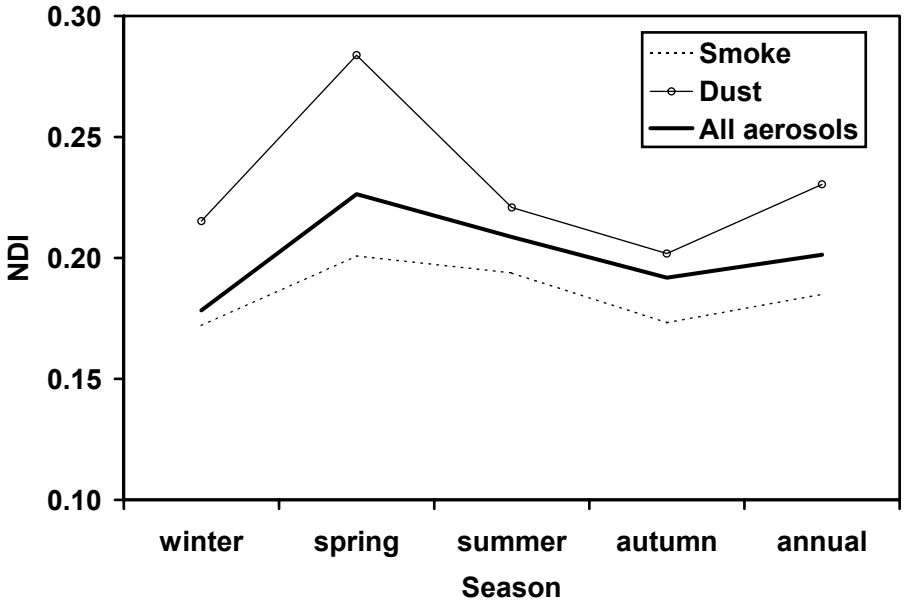

Fig. 10. Net diabatic impact of aerosols at the ARM Southern Great Plains Central Facility.

ACPD
3, 2353–2391, 2003